The Journal of Physical Chemistry A

 VOLUME 103, NUMBER 33, AUGUST 19, 1999

FEATURE ARTICLE

Photoexcitation, Ionization, and Dissociation of Molecules Using Intense Near-Infrared Radiation of Femtosecond Duration

Robert J. Levis*,† and Merrick J. DeWitt

Department of Chemistry, Wayne State University, Detroit, Michigan 48202

Received: November 30, 1998; In Final Form: June 18, 1999

The coupling mechanism between an intense ($\sim 10^{13}$ W cm^{-2}, 780 nm) near-infrared radiation field of duration 50−200 fs with molecules having 5−50 atoms is considered in this article. In general, the interaction of intense radiation fields with molecules can result in both electron emission and subsequent dissociation. For the laser excitation scheme employed here, intact ions are observed in addition to dissociative ionization channels for all classes of molecules investigated to date. An excitation mechanism is considered where the electric field of the laser mediates the coupling between the radiation and the molecule. This field-induced ionization is compared with the more common frequency-mediated coupling mechanism found in multiphoton processes. Measurements of intense-laser photoionization probability are presented for several series of molecules. An outline of our structure-based model is presented to enable calculation of relative tunneling rates and prediction of the laser−molecule coupling mechanism. The relative ion yields for various series of hydrocarbon molecules are found to be in good agreement with that predicted by the structure-based tunnel ionization model. Measurements of photoelectron kinetic energy distributions also suggest that the ionization phenomena proceed to a large degree through a field-mediated excitation process. The photoionization/dissociation products are measured in an ion spectrometer and are interpreted in terms of a competition between electronic excitation and energy transfer to nuclear degrees of freedom. Evidence for field-induced dissociation is presented.

I. Introduction

The interaction of ultrafast, intense radiation ($\sim 10^{13}$ W cm^{-2}) with polyatomic gas-phase molecules will be considered in this article. In this intensity regime, the amplitude of the electric field vector of the radiation is on the order of 1 to 5 V/Å. Since this is on the order of the electric fields binding valence electrons to molecules, we might anticipate that the electric field of the laser will play an important role in the radiation−molecule interaction at high laser intensity. The interaction of intense lasers with gas-phase atoms and molecules has led to the observation of many novel phenomena including X-ray generation from high harmonics,[1] above threshold ionization,[2] above threshold dissociation,[3] multiple electron emission,[4] and molecular ionization using near-infrared laser pulses.[5] The focus of this paper will be restricted to the intensity regime that leads to single electron emission from polyatomic molecules. This area is of interest because the coupling mechanism appears to be universal; one excitation wavelength leads to ionization of a wide variety of molecules. The area is also of interest because the ionization process leads to far less photodissociation than one might expect at such high photon densities.

The coupling between a radiation field and a molecule is commonly described using first-order time-dependent perturbation theory. As the intensity of the laser field is increased, however, lowest-order perturbation theory becomes insufficient, and one must include higher order corrections. Corrections to very high order are possible only for highly symmetric systems such as the hydrogen atom. In the case of polyatomic molecules,

* To whom correspondence should be addressed.
† Camille Dreyfus Teacher Scholar and Sloan Fellow.

10.1021/jp984543v CCC: $18.00
Published on Web 07/30/1999

these calculations rapidly become difficult or impossible. In the intense field regime, one must account for the perturbation of the molecular wave function by the amplitude of the electric field of the radiation. The amplitude of the electric field, E_0, is related to the intensity of the radiation, I, by

$$E_0 = \left(\frac{2I}{\epsilon_0 c}\right)^{1/2} \quad (1)$$

where c is the speed of light and ϵ_0 is the vacuum permittivity. For example, at 10^6 W cm^{-2} (typical for nanosecond lasers), the magnitude of E_0 is 2.7×10^{-4} V Å^{-1} and is in the weak field limit, while at 10^{14} W cm^{-2}, the magnitude of E_0 is 2.7 V Å^{-1} and is in the strong field limit. As the electric field of the laser approaches that binding valence electrons to the molecule, perturbation theory breaks down and computationally intensive numerical procedures must be developed to accurately model the time-dependent quantum mechanics.[6] The high electric fields perturb molecular electronic states causing substantial state mixing and field-induced avoided-curve crossings.[7] Another manifestation of the perturbation is evident in massive Stark shifting of intermediate and high-lying eigenstates both in and out of resonance.[8,9] All of these complications make accurate calculations of the behavior of even the simplest diatomic and triatomic species (those containing a small number of electrons) nearly intractable. To treat complex molecular systems, a large number of simplifying assumptions must be allowed.

At even higher fields, one can enter the regime of field ionization where the rate of both tunnel ionization and barrier suppression ionization may coexist with or supersede the rate of multiphoton ionization. The two distinct regimes for coupling of the intense radiation with atomic or molecular systems, multiphoton and field excitation (encompassing both tunnel and barrier suppression ionization), are shown in Figure 1. Keldysh[10] developed a theory to delineate the boundary between multiphoton ionization (MPI) and field ionization processes. As is described in detail in section III.3, an adiabaticity parameter (called γ and based on the zero range approximation) is defined for this purpose by comparing a calculated tunnel frequency to the laser frequency. The adiabaticity parameter essentially determines whether tunnel ionization is feasible or whether multiphoton ionization must occur. The Keldysh treatment of intense laser−atom interactions has been confirmed in numerous subsequent theoretical[11,12] and experimental investigations.[13−16] We have developed a model that accounts for the extended electronic structure found in polyatomic molecules in order to more accurately predict the coupling mechanism.[17] In our structure-based model, the electrostatic potential is not approximated by the zero range potential but rather by a one-dimensional potential based on the actual wave function of the molecule.[18] The structure-based potential can then be employed to define a modified adiabaticity parameter, termed $\gamma(\psi)$, and can be employed in calculations of relative ionization probability.

The ionization of molecular species interacting with intense laser pulses is more complex than the atomic case because energy may be channeled into nuclear degrees of freedom. The majority of the experiments involving molecules and high-intensity lasers have been performed using diatomic molecules.[7,19−24] Molecular hydrogen has been investigated most thoroughly,[8,25−27] and a charge resonance enhanced ionization (CREI) model has been shown to account for high-intensity ionization processes in this molecule.[6,28,29] In this model, the electric field of the laser perturbs the bond length of H_2, and at some elongated bond distance, the molecule's ionization rate

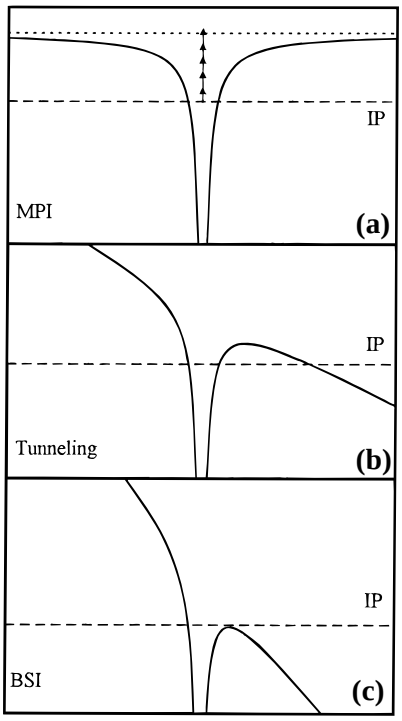

Figure 1. Depiction of the limiting paradigms for the interaction of atoms with radiation. (a) represents the frequency-mediated multiphoton coupling mechanism where n photons couple into an atom to produce ionization. (b) represents the field-mediated coupling mechanism where the electric field of the laser perturbs the electrostatic potential of the atom to allow tunnel ionization. (c) represents the field-mediated coupling mechanism of barrier suppression ionization.

reaches a maximum. The ionization is due to a combination of static field barrier suppression and dynamic localization of the electron by the laser field. For more complex diatomic and triatomic systems, essentially two regimes of excitation have been investigated. Under the conditions of infrared (10 μm) excitation, molecules such as N_2,[19] O_2,[23] CO,[23] NO,[23] and I_2[23] have been found to tunnel ionize. At shorter wavelengths, principally in the visible, molecules such as O_2,[22] Cl_2,[30] I_2,[32] CO_2,[31] C_2H_2,[33] C_2H_4,[33] C_3H_4,[34] and C_3H_8[34] have been found to undergo a similar excitation mechanism at laser power densities near 10^{15} W cm^{-2}. In the case of the intense visible laser excitation mechanism, a molecule begins to align (to some degree) with the electric field, then elongate, and, at some optimal bond distance correlating to the electric field strength of the laser, ionize rapidly. This sequence of events leads to a Coulomb explosion with the resulting kinetic energy of the fragments being lower than that expected for ionization at the equilibrium bond distance. Because of the extremely high laser pulse intensities employed, 10^{15} W cm^{-2}, multiple ionization and substantial fragmentation is observed in these studies.

The laser pulses considered in this paper have duration on the order of molecular vibrations (100 fs) in addition to the associated high intensity. This rapid time scale results in one of the most remarkable features of these experiments: that photoionization can be induced with limited corresponding photodissociation in a variety of molecules using a single excitation wavelength. At least two dissociation mechanisms must be overcome to produce intact ionization. The first such mechanism may be called absorption−dissociation−ionization[35] (ADI) or the ladder switching mechanism. As one example of this mechanism, consider the scenario depicted in Figure 2a. In this example, the polyatomic ABC absorbs one (or more) photon(s) of energy $h\nu$ to reach a repulsive potential energy

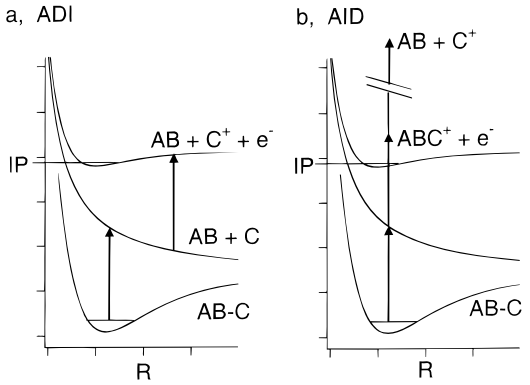

Figure 2. Schematic of two mechanisms for dissociative ionization. (a) represents the mechanism of absorption dissociation and ionization (ADI) where the molecule first dissociates and the fragments proceed to absorb additional photons to ionize. (b) represents the mechanism of absorption, ionization, and dissociation (AID) where the molecule first ionizes and the ion absorbs additional photons to subsequently dissociate.

surface. On this potential, the molecule will dissociate on a short time scale, on the picosecond to subpicosecond time scale. Depending on the laser pulse duration, the dissociated fragments can then absorb additional photons to ionize and produce a mass spectrum that may consist of only fragments of the original molecule. To circumvent ADI, the laser intensity must be increased sufficiently that intact ionization occurs on a time scale that is faster than the neutral dissociation time scale. Unfortunately, in the case of longer duration laser pulses (picosecond to nanosecond), a molecular ion produced early in the laser pulse is capable of absorbing additional photons that will invariably induce subsequent dissociation. This second mechanism for dissociative ionization is called absorption−ionization−dissociation[36] (AID) or the ladder climbing mechanism. An example is shown in Figure 2b where molecule ABC absorbs one (or more) photon(s) to produce ABC^+. Subsequent absorption of photons leads to dissociation of ABC^+ to one or more ion fragments. As in the case of ADI, the mass spectrum resulting from AID often consists of only fragment species.

The duration of the laser pulse employed for weak field, resonant multiphoton excitation does afford some degree of control over the quantity of energy deposited into nuclear modes prior to ionization. Experimental observation of reduced energy transfer from electronic modes to nuclear modes can be inferred from an increase in ionization probability and a corresponding decrease in the photodissociation probability with decreasing pulse duration of the excitation laser. Early investigations by El-Sayed and co-workers demonstrated reduced photodissociation/ionization of molecules using picosecond excitation schemes in comparison with nanosecond excitation.[38−40] Reilly and co-workers[41,42] demonstrated that picosecond pulses have higher photoionization yield than nanosecond pulses for molecules with rapid excited-state relaxation. Castleman and co-workers[43] and Gerber and co-workers[44] observed no change in the relative intensities of the ionized molecular and atomic clusters as the power density of a femtosecond duration laser pulse was increased. Similar nanosecond experiments demonstrated markedly increased fragmentation at higher laser power densities.[45] Imasaka noted enhanced ionization efficiency for adenine[46] and halogenated benzenes[47] upon femtosecond excitation. Benninghoven and co-workers[48] and Grotemeyer and co-workers[49] have compared the ionization efficiency using nonresonant femtosecond and nanosecond radiation excitation of large molecules. Both groups found enhanced ionization efficiency and decreased dissociation yield using shorter time scale excitation pulses. Stuke and co-workers also observed reduced fragmentation using picosecond ionization processes for $Se(CH_3)_2$, $Te(CH_3)_2$, and $CH_3TeTeCH_3$.[50−52] Ledingham has demonstrated that multiphoton excitation of NO_2 using 300 fs pulses increases the yield of intact ion by a factor of 60 compared to nanosecond excitation.[53] Gerber and co-workers also demonstrated that intact $Fe(CO)_5^+$ was obtained using femtosecond excitation at 400 nm, while nanosecond excitation at 337 nm provided only Fe^+ signal.[54] Ultrafast multiphoton ionization has been employed to observe chemical reactions occurring in real time.[55] In the case of visible/UV MPI, shorter pulse duration enhances molecular ion signal because ionization rates can begin to compete favorably with dissociation rates. In each of these examples, both AID and ADI can contribute to the dissociation−ionization channel in the nanosecond case. In the case of femtosecond excitation, the molecule does not have time to undergo substantial nuclear motion during the peak in the radiation intensity, and thus ADI may be reduced or eliminated. This does not mean that dissociation is completely eliminated using femtosecond excitation. For instance, dissociation during femtosecond excitation may occur by subsequent excitation of the neutral complex well above the ionization potential, i.e., the ladder climbing mechanism.

In 1995, this laboratory reported the use of intense near-infrared laser radiation of femtosecond duration to ionize large polyatomic molecules,[5] in many cases with little accompanying dissociation.[17,18,56−58] This experiment is intrinsically different from the ultrafast MPI work just described. The ionization method employs no low-lying intermediate states for excitation; hence the excitation is essentially nonresonant. The ionization also occurs in the strong field regime where the laser pulse significantly perturbs the eigenstates of the neutral molecule. After our initial report, a number of groups have published complementary investigations using the same near-IR ionization method. Willey et al. reported the femtosecond ionization of $Cr(CO)_6$.[59] Ledingham et al. reported the ionization of NO_2 and other heteroatomic molecules.[60,61] Baumert and co-workers used near-IR ionization to probe the photodissociation of $Fe(CO)_5$.[62] Trushin and co-workers used near-IR ionization to probe the time-dependent photochemistry of cyclohexadiene[63,64] and $Cr(CO)_6$.[65] Castillejo et al. have investigated the intense laser ionization of hydrocarbons.[66] Phenomenologically, it is clear from these experiments that ultrafast, intense laser pulses lead to enhanced molecular ion signal in comparison to nanosecond excitation. Determining the precise mechanisms of such interactions and evaluating the practical limits of such excitation−ionization schemes has not yet been accomplished.

II. Experimental Section

The experiments presented in this article employ a solid-state femtosecond oscillator based on the Ti:sapphire crystal.[67] The relatively simple Ti:sapphire oscillator can emit sub-100 fs pulses tunable from 1100 to 700 nm at a few nanojoules per pulse. The system employs two oscillators, one with a pulse duration of 135 fs and another with a pulse duration of 30 fs. The pulses from either oscillator are too weak to produce detectable photoionization, so regenerative amplification in a second Nd:YAG pumped Ti:sapphire crystal is used to provide a gain of 10^6.[68] The process includes a grating pulse expander which effectively stretches the pulses in time from ∼100 fs to ∼100 ps. These pulses are then directed into a Nd:YAG pumped, Ti:sapphire regenerative amplifier. Single pulses are amplified $>10^6$ times in the regenerative amplifier and are then switched out to a parallel grating pair where the pulse is compressed back

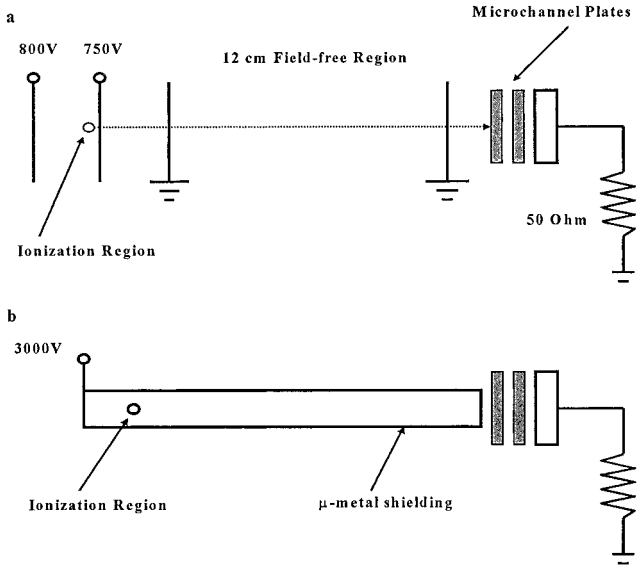

Figure 3. (a) Schematic of the time-of-flight mass spectrometer employed to measure the resulting mass spectra of ions produced by intense near-infrared excitation. (b) Schematic of the photoelectron spectrometer.

to the initial short pulse duration. The regeneratively amplified femtosecond laser is capable of producing 0.5 mJ of 170 fs light at 780 nm. The system can operate at up to 10 Hz, and the rate is restricted by the repetition rate of the Nd:YAG pump laser. The final laser intensity is altered by placing quartz coverslips in the beam path. This produces a calibrated and repeatable decrease in the laser intensity of 5% per coverslip.

The femtosecond laser is focused into a time-of-flight mass spectrometer to perform ion detection. The system employs a 0.5 m linear drift tube and ions are accelerated to 800 eV in a dual slope extraction region as shown in Figure 3a. Ions are detected using a microchannel plate stack. Sample introduction is accomplished via a pulsed valve or by allowing solid samples to freely sublime into the gas phase. The pressures employed for these experiments range from 10^{-5} to 10^{-7} Torr. The photoelectron spectra were collected using a linear drift tube with μ-metal shielding and a drift length of 29.5 cm, as shown in Figure 3b. The tube was floated to -3 keV, and the electrons were also detected using a microchannel plate assembly. The base pressure of the chamber was 3×10^{-7} Torr, and the molecules were admitted into the chamber effusively or were allowed to sublime directly into the vacuum. The signal from both spectrometers was recorded using a 2 GHz digital oscilloscope. The resulting time-of-flight spectrum was then transferred to a 486 computer via GPIB interfacing for data storage and display.

III. Results and Discussion

III.1. General Phenomenology and Overview. The general experimental observation resulting from interaction of the 780 nm 170 fs laser pulse with a polyatomic molecule is presented in the series of mass spectra displayed in Figure 4. The ion time-of-flight mass spectra are shown for the molecules benzene, dichlorodifluoromethane, and trimethylaluminum after the ground state, gas-phase molecules have interacted with the intense 780 nm radiation. The spectra demonstrate that one can efficiently couple the near-infrared radiation into the molecules and that the coupling mechanism results in substantially less dissociation of the ion product than is observed using nanosecond excitation. In the case of benzene, efficient ionization can be produced using

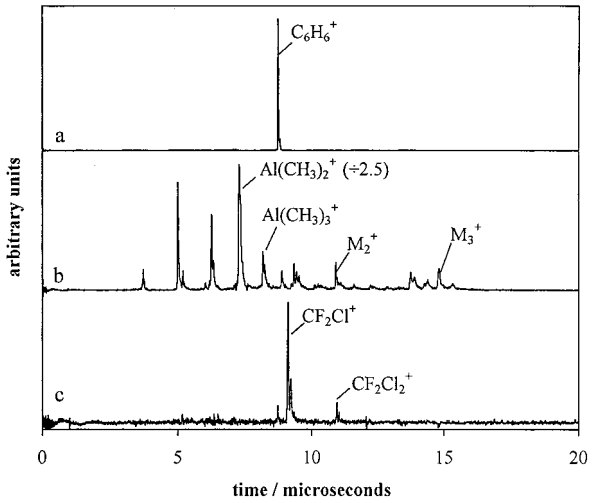

Figure 4. Time-of-flight mass spectra for (a) benzene, **(**b) trimethylaluminum, and (c) CCl_2F_2, taken using 780 nm excitation with a laser pulse intensity of 3.8×10^{13} W cm^{-2} (170 fs pulse duration).

nanosecond resonant excitation methods in the near-UV ($\sim 10^6$ W cm^{-2}), but nanosecond nonresonant excitation using visible or near-IR wavelengths requires much higher power densities ($> 10^{10}$ W cm^{-2}) and results in nearly complete dissociation of the observed products because of AID. For the molecules dichlorodifluoromethane and trimethylaluminum, intact ions cannot be produced using any multiphoton or resonant multiphoton excitation process utilizing nanosecond duration laser pulses because ADI occurs on repulsive intermediate potential energy surfaces. In the case of intense, 170 fs, near-infrared excitation of the organometallic molecule, one observes fragmentation products as well as intact molecular ion and multimers of the intact ion extending up to M_3^+ (Figure 4b). Similar 780 nm excitation results in fragmentation of the chlorofluorocarbon, but there is a measurable quantity of intact molecular ion produced, as shown in Figure 4c.

From this qualitative view of the photoion measurements, two questions are readily apparent. The first question concerns the mechanism of coupling between the radiation and a given polyatomic molecule. Apparently, the precise frequency matching conditions necessary in resonance-enhanced MPI experiments are not required for the intense near-infrared ionization experiment.[5,17,18,54−66] What then is the mechanism of coupling between the intense laser pulse and the molecule? The second question concerns the limited fragmentation yield measured at 10^{13} W cm^{-2}, even though one might expect complete dissociation through AID using such intense laser pulses. What are the operative mechanisms of photodissociation during the intense laser excitation? Our investigations of these two questions form the remainder of this paper. To address the mechanism of coupling between the intense near-IR radiation field and a polyatomic molecule, we have performed both photoion and photoelectron measurements. Section III.2 will present an overview of the mass spectroscopic measurements, the procedure used to extract of relative ionization probabilities, and some pertinent theory used to interpret the measured orders. Relative ionization probabilities have been measured for several series of molecules as a function of laser intensity to determine the effect of molecular structure on the field−molecule coupling process. The relative ionization probabilities are not consistent with current zero range or Coulombic models for atomic ionization in high fields. Hence, in section III.3, we present our structure-based model for intense laser ionization of polyatomic molecules. This model is based on the determination of an

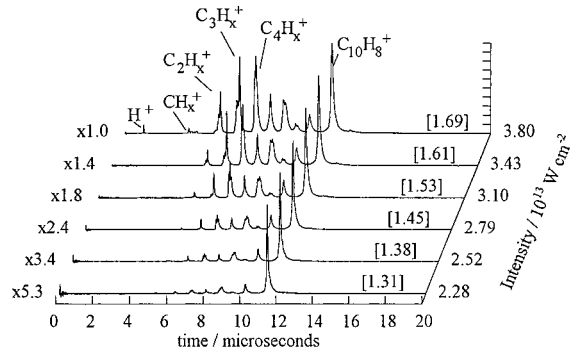

Figure 5. Time-of-flight mass spectra for naphthalene ($C_{10}H_{12}$) excited using 780 nm, 170 fs laser pulses as a function of laser intensity from 1 to 4 × 10^{13} W cm^{-2}. The spectra are normalized and the relative scalar for each spectrum is shown to the left of the respective trace. The number in brackets represents the electric field strength in V Å^{-1}.

optimal one-dimensional electrostatic potential and a field-mediated coupling mechanism. The predictions of the model are compared with the relative ion yield measurements. To further test the predictions of the structure-based model, we present photoelectron spectroscopy measurements for benzene, naphthalene, and anthracene in section III.4. Finally, in section III.5, we present our observations and speculations on the mechanism of dissociation using intense near-infrared laser pulses.

III.2. Ion Spectroscopy. We first consider the photoionization/dissociation spectra as a function of molecular structure and laser intensity. The mass spectra for naphthalene are reproduced in Figure 5 upon interaction with a 780 nm laser beam having a pulse duration of 170 fs with intensity ranging from 1 to 3.8 × 10^{13} W cm^{-2}. Such an experiment contains several complementary pieces of information. First, the total ion yield can be plotted as a function of the laser intensity to determine the order of the ionization process. The total ion yield is obtained by integrating the ion current in a given spectrum. For the case of naphthalene, the logarithm of this sum is plotted as a function of the logarithm of the laser intensity as shown in Figure 6. The general features of Figure 6 are common to all of the molecules studied in this laboratory to date. A linear dependence is observed in the log−log plot over a change in ion signal of more than 2 orders of magnitude. In the multiphoton excitation mechanism, the slope is related to the order of the ionization process through the following expression:

$$Y = \sigma_n I^n \tag{2}$$

where Y is the ion yield, σ_n is the nth-order cross section, and I is the laser intensity.[69] Evaluating the logarithm of this equation linearizes the data, and the slope of the line is the order of the process. In the case of naphthalene, the slope is 8.5. In nonresonant multiphoton ionization, the order multiplied by the quantum energy of the photon always exceeds the ionization potential by less than one quantum of photon energy. For naphthalene, the order multiplied by the photon energy returns a value of 13.9 eV, which is 5 eV above the vertical ionization potential. Given the photon energy of 1.59 eV, this suggests that at least three additional photons are absorbed during the ionization process. The observation of excessively high orders in the 780 nm ionization of polyatomic molecules is one common feature in the measurements that we have performed on many different molecules.

There are several possibilities to explain the excess order of the ionization process. The additional photons absorbed during

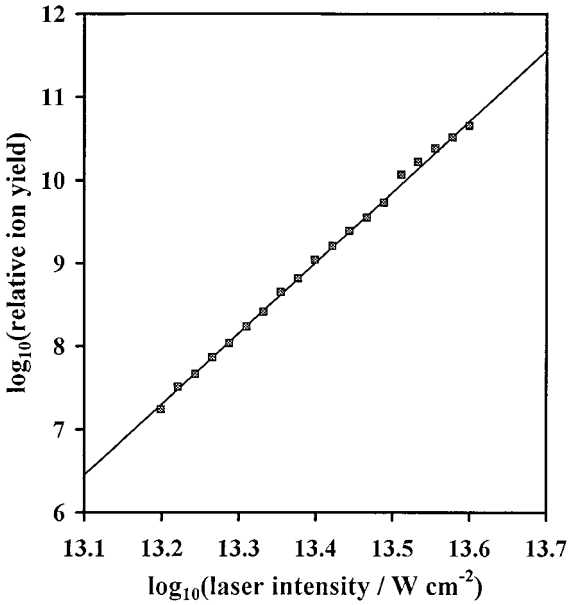

Figure 6. Plot of the logarithm of the total ion intensity in a given naphthalene spectra as a function of the logarithm of the laser intensity employed for ionization. A least-squares fit through the data points is shown as the solid line. The slope of this line is 8.5. In the MPI model, this is equivalent to the order of the ionization process and would signify an ionization process requiring 12.9 eV.

the ionization process may be due to an increase in the ionization potential by an amount nearly equal to the ponderomotive potential of the intense laser pulse. This effect can be illustrated by considering the interaction of an electromagnetic field with a free electron. In the velocity gauge, the Hamiltonian for this system is given by

$$H = \frac{\left[\mathbf{p} - \frac{e}{c}\mathbf{A}(\mathbf{x},t)\right]^2}{2m_e} \tag{3}$$

where **p** is the momentum of the electron and **A** is the vector potential of the radiation field. Upon expansion of the Hamiltonian one obtains

$$H = \frac{p^2}{2m_e} - \mathbf{p}\cdot\frac{e}{2m_e c}\mathbf{A}(\mathbf{x},t) - \frac{e}{2m_e c}\mathbf{A}(\mathbf{x},t)\cdot\mathbf{p} + \frac{e^2}{2m_e c^2}\mathbf{A}^2(\mathbf{x},t) \tag{4}$$

The first term is the kinetic energy of the electron. The second and third terms describe the time-dependent interaction of the electron with the radiation field. Averaged over an integral number of cycles of the radiation field one is left with:

$$\langle H\rangle = \frac{p^2}{2m_e} + \frac{e^2\mathbf{A}^2(\mathbf{x})}{4m_e c^2} = T + U_p(\mathbf{x}) \tag{5}$$

The time-averaged Hamiltonian becomes the sum of the average drift kinetic energy (T) and the average kinetic energy due to the electron moving in the vector potential [$U_p(\mathbf{x})$]. The latter quantity is equal to the ponderomotive potential of the radiation field and refers to the wiggle or quiver motion[70] of the electron in the oscillating field. In the length gauge, Kibble[71] has shown that the ponderomotive potential is given by the average kinetic energy of the electron accelerated by the electromagnetic field,

$$U_p = \frac{1}{2} m_e \langle \dot{r}^2 \rangle = \frac{e^2 {E_0}^2}{4 m_e {\omega_0}^2} \tag{6}$$

where r is the position of the electron, E_0 is the amplitude of the plane wave $\mathbf{E} = E_0 e^{i\omega_0 t}$ and ω_0 is the angular frequency. To understand the increase in ionization potential, we must consider the time-dependent Hamiltonian as shown in eq 4. According to this Hamiltonian, all states are raised in energy by the $\mathbf{A}^2$ term (which gives rise to the ponderomotive potential) of the radiation field.[72] The increase in ionization potential results from the fact that the ground state is also decreased in energy by nearly U_p via the second-order expansion term of the $\mathbf{A}\cdot\mathbf{p}$ portion of the time-dependent Hamiltonian in the long wavelength limit.[70] Thus, because states near the ionization potential have almost no downward $\mathbf{A}\cdot\mathbf{p}$ shift, the ionization potential is observed to increase by a value approximately equal to U_p. This approximation applies only for deeply bound ground states having no resonances lying within several electronvolts. In a more classical sense, one can think of the increase in IP as arising from induced polarizability of the ground state and states near the ionization potential. Strongly bound electrons experience a shift in energy due to the ponderomotive potential as given by[73]

$$\Delta E = \left(\frac{\omega_0}{\omega_{IP}}\right)^2 U_p \tag{7}$$

where $h\omega_{IP}/2\pi$ represents the ionization potential of the state. For deeply bound ground states the field-induced polarization is small, hence the shift is small. High-lying Rydberg states are observed to shift upward in energy by a value of approximately U_p,[70] giving rise to the effective increase in ionization potential. For the conditions employed in this experiment, the increase in the ionization potential at maximum intensity is on the order of one to two photons and this shift may account for the increased order over that expected for the field-free ionization potential. It should be pointed out that it is not clear what orders are to be predicted from field ionization mechanisms in the short pulse limit.

An alternative rationalization for the high order of the ionization process would be the presence of above threshold ionization during the excitation and emission process. Above threshold ionization (ATI)[2] involves the absorption of additional photons over and above the lowest number required for ionization. In this case, the expected N^{th} order dependence (determined by IP/$h\nu$) may increase because $N + 1$, $N + 2$, $N + 3$, ... processes contribute to the measured ion order. The ATI phenomenon is clearly delineated by well-defined peaks in the photoelectron spectrum separated by $h\nu$ above those expected from lowest order perturbation theory. Such processes are commonly observed in high-intensity photoelectron experiments.[15,70] As will be seen, there is evidence for ATI in benzene, but in naphthalene and anthracene, there is little ATI current present. It is important to note that both the shift in the ionization potential and the presence of ATI arise from the strong field interaction of an intense laser pulse with an atom or molecule. Since this interaction can only be understood through the deployment of approximate models, there is considerable room for improvement in the understanding of intense laser phenomena for molecular systems.

A comparison of the relative photoionization yields at maximum laser intensity for a number of hydrocarbon molecules investigated in this laboratory reveals that the ionization probability increases exponentially as the ionization potential decreases. The relative ionization probability is plotted as a function of IP for benzene, toluene, ethylbenzene, *n*-propylbenzene, naphthalene, phenanthrene, and anthracene in Figure 7 as the open squares. Note that in this figure all of the ionization probabilities are normalized to that observed for benzene. This exponential increase must be due to more than the fact that the ionization potential decreases across this series. A simple IP dependence is assumed in an expression for ionization rate that is based on Keldysh's original derivation. Ammosov, Delone, and Krainov (ADK)[74] derived an expression for the ionization frequency, w:

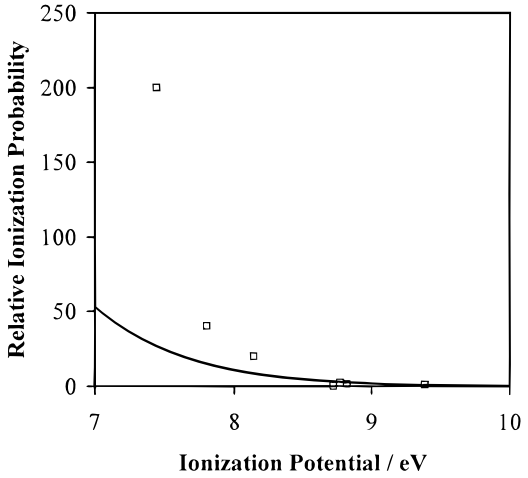

Figure 7. Plot of the relative ionization probability for excitation using 3.8×10^{13} W cm^{-2} 780 nm laser radiation as a function of the ionization potential of the molecules anthracene, phenanthrene, naphthalene, *n*-propylbenzene, ethylbenzene, toluene, and benzene (ordered from lowest IP to highest). The solid line represents the ionization probabilities calculated using the ADK theory for a structureless atom as outlined in the text.

$$w = \left(\frac{3e}{\pi}\right)^{3/2} \frac{Z^2}{3n^{*3}} \frac{2l+1}{2n^* - 1} \left[\frac{4eZ^3}{(2n^* - 1)n^{*3}F}\right]^{2n^* - 3/2} \exp\left[\frac{-2Z^3}{3n^{*3}F}\right] \tag{8}$$

where Z is the nuclear charge, l is an angular momentum term, $n^* = Z/(2\mathrm{IP})^{1/2}$, and F is the field strength of the laser. In ADK theory, it is the ionization potential of the system and the field strength of the radiation that exclusively govern the photoionization rate (i.e., laser frequency is not accessible in this theory). The relative ionization frequencies calculated using the ADK method are shown by the solid line in Figure 7, assuming that $l = 1$ for each of the molecules investigated. The angular momentum appears only in a scalar term. We assume that $l = 1$ for all calculations so that all values are guaranteed to be correct to within a factor of 3 for angular momentum values varying from 0 to 4. Over this range of ionization potentials, the structureless atom model predicts a weak dependence of the ionization probability on the ionization potential. The predictions of the ADK model rapidly diverge from the experimentally measured relative ionization probabilities for larger polyatomic molecules. A log−lin plot of the data reveals that the difference between the ADK and measured values is more than a constant factor; the slopes are markedly different. We conclude from this comparison that if a field ionization model is to be applied to fit the data obtained for the molecules investigated here, a simple atomic model is probably not the most appropriate model for the coupling mechanism. Thus, we sought to introduce a model that would account for the effect of the structure of a molecule on the ionization probability. It

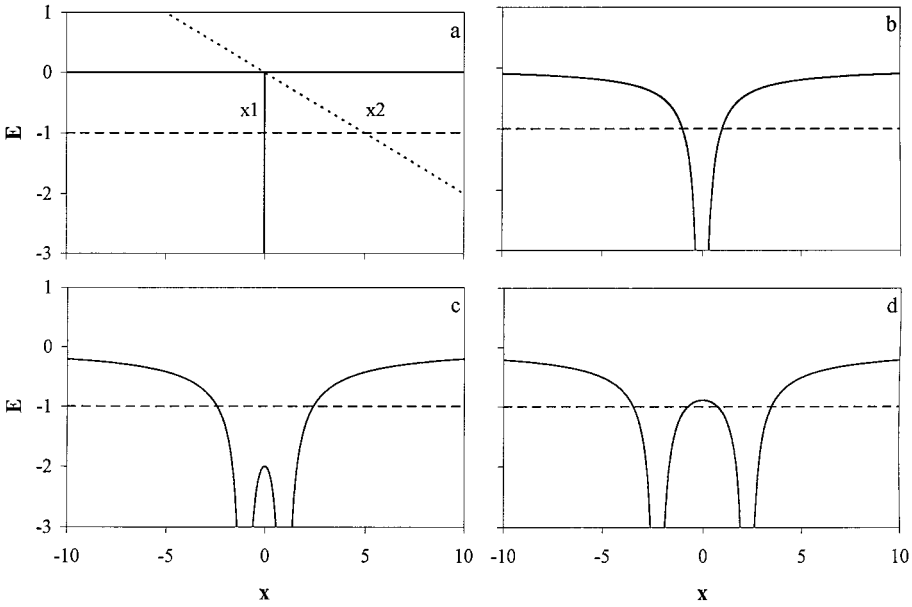

Figure 8. Various electrostatic potentials used for theoretical calculations: (a) the zero range potential which simply accounts for ionization potential, the dotted line denotes the superposition of a static electric field giving rise to the classical turning points at x_1 and x_2; (b) the Coulomb potential used for atomic calculations; **(**c) a diatomic potential where the ionization potential resides above the inner electrostatic barrier; **(**d) a diatomic potential where the ionization potential resides below the inner electrostatic barrier. In each case, the dashed line represents the IP of the system.

should be noted that, in comparison to experimental values, both ADK and the structure-based models converge at high values of IP so that previous studies[13,14] of molecules with relatively high IP are found to be consistent with ADK theory.

III.3. Structure-Based Model for Near-IR Photoionization of Molecules. To develop a more accurate picture of the intense IR−molecule interaction, we have focused on incorporating ab initio molecular electrostatic potentials into a quasistatic model.[17,18] Molecular potentials are introduced to model the electronic delocalization present in polyatomic molecules, and the quasistatic picture is employed because time-dependent high-order photoabsorption cross sections are impossible to calculate for large systems at this time. For the case of atomic and diatomic systems, the zero range model has proven a useful predictor of the ionization mechanism.[11−14] However, the delocalized nature of electronic orbitals in polyatomic molecular systems will limit the applicability of zero range models. For example, a simple calculation of the Keldysh adiabaticity parameter for molecules having an ionization potential on the order of 10 eV for our laser conditions returns a value on the order of 4. This suggests that MPI would be the dominant coupling mechanism regardless of the markedly changing electronic structure. As we have shown, the adiabaticity parameter can range from ∼1 to 0 (zero denoting barrier suppression ionization) for identical laser conditions when molecular structure is incorporated.[17] An adiabaticity parameter less than one suggests that field ionization would be the dominant coupling mechanism. As will be seen, photoelectron measurements are consistent with a field ionization mechanism for the molecules and laser conditions employed in our investigations.

The structure-based model seeks to account for the fact that polyatomic molecules have delocalized electronic orbitals that are not well described by zero range or Coulomb potentials (see Figure 8). *To account for the extended structure of polyatomic molecules we determine a characteristic length for interaction with the laser electric field. The optimal length employed in the structure-based tunneling model is derived from that one-dimension potential in the molecular wave function having the greatest distance between outer classical turning points at the ionization potential of the neutral.* To summarize the structure-based model, we begin with an ab initio geometry optimization of the neutral molecule. The neutral geometry is then used to calculate the wave function of the singly charged positive ion using frozen coordinates. To parallel the original Keldysh derivation, we require a one-dimensional electrostatic potential. There are an infinite number of possible one-dimensional potentials in a polyatomic wave function, and each may be unique. Our model seeks to employ the optimal one-dimensional electrostatic potential, and this requires determination of an origin and orientation for an axis within the wave function. In the structure-based model, the optimal potential corresponds to the one-dimensional electrostatic potential having maximum distance between classical turning points defined at the neutral ionization potential. The optimal potential is employed in a calculation of the structure-based modified adiabaticity parameter, $\gamma(\psi)$, and the determination of the relative tunneling rate via the Wentzel−Kramers−Brillouin (WKB) method.

To introduce the structure-based calculation of $\gamma(\psi)$ and the relative tunneling probability, we begin with a consideration of simpler calculations using the zero range and Coulomb potentials. In the Keldysh treatment, a zero range potential, as shown in Figure 8a, is employed to model the atomic potential during interaction with the radiation. The zero range potential is a δ-function having a state at the atomic ionization potential (IP). The zero range potential perturbed by a strong external field defines two classical turning points (an inner and an outer) for electron motion. These turning points are denoted by x_1 and x_2 in Figure 8a. The length of the barrier between these turning points is

$$l = \frac{\mathrm{IP}}{eE_0} \tag{9}$$

where e is the charge of an electron. The average kinetic energy of an electron is equal to IP according to the virial theorem and the average velocity of the electron is then

$$\langle v \rangle = \left(\frac{2\mathrm{IP}}{m_e}\right)^{1/2} \tag{10}$$

where m_e is the mass of an electron. From the average velocity, one can determine the average time for an electron to cross a barrier of length l. This is the tunneling time. The tunneling frequency, ω_t, is the inverse of the tunneling time and is given by

$$\omega_t = \frac{\langle v \rangle}{l} = \frac{\sqrt{2}eE_0}{\sqrt{\mathrm{IP}m_e}} \tag{11}$$

The adiabaticity parameter, γ, is then defined as the ratio of the laser frequency to the tunneling frequency via

$$\gamma = \frac{\omega_0}{\omega_t} = \sqrt{\frac{2\mathrm{IP}m_e\omega_0^{\,2}}{e^2E_0^{\,2}}} \tag{12}$$

where ω_0 is the laser frequency and ω_t is the tunnel frequency. If $\gamma \gg 1$, there is insufficient time for tunneling to occur and the MPI process dominates; if $\gamma \ll 1$, tunnel ionization occurs. For the case of the zero range potential, the values of IP, E_0, and the laser frequency completely determine the value of the adiabaticity parameter and therefore the predicted ionization mechanism.

A more realistic model is obtained upon incorporating a Coulomb potential (Figure 8b) into the adiabaticity and tunnel rate calculations. More sophisticated potentials require consideration of both the origin and location of the one-dimensional axis that determine the direction of the external electric field. In the case of the Coulomb potential, the only logical choice for the origin position is at the center of the potential. Choice of axis orientation is also simplified in the case of the Coulomb potential due to its one-dimensional nature. In the presence of an external electric field, a barrier is again formed with well-defined inner and outer turning points. These provide a length, tunnel time, and tunnel frequency in parallel with the zero range potential. The resulting tunnel frequency can again be employed in eq 12 to determine a modified adiabaticity value.

A comparison of the Keldysh and Coulomb-based adiabaticity values are shown for xenon and the molecules N_2, benzene, naphthalene, and anthracene in Figure 9 (as are the values for the structure-based model to be detailed subsequently). As can be seen there are several important distinctions between the zero range and Coulomb derived adiabaticity parameters. The first distinction is that the values for the Coulomb-based model are always lower than those obtained by the zero range definition, as has been shown previously.[17] This results from the decreased barrier length in the Coulomb model. The structureless zero range potential has an inner barrier that is located at the origin for all field strengths and for systems of any IP. The Coulomb potential has an inner barrier which is located at some distance from the origin. The distance from the origin increases as the electric field strength is increased and this gives rise to a length that approaches zero much more rapidly than in the zero range model. The outer barrier decreases with increasing electric field strength in either model. The distance from the origin to the inner barrier also increases as ionization potential decreases at constant field strength. Conversely, the outer barrier decreases with decreasing ionization potential at constant field strength. These correlated effects on the inner and outer barrier position lead to a dramatic reduction in the barrier length (with respect to the zero range model) for species with relatively low

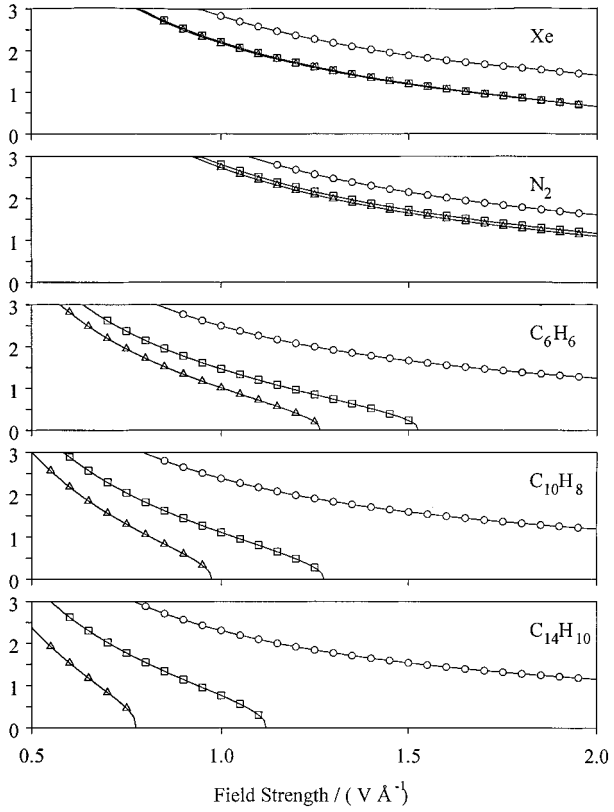

Figure 9. Plot of the adiabaticity parameter as a function of electrostatic potential (circles are zero range, squares are Coulomb, and triangles are ab initio potentials) for **(**a) Xe, (b) N_2, (c) benzene; (d) naphthalene, and (e) anthracene.

ionization potentials ($\leq$10 eV). Since the tunneling frequency in the definition of the adiabaticity parameter depends on the barrier length, we conclude that the structure-based models can have a dramatic effect upon the interpretation of field ionization mechanisms. The second distinction is that, while the zero range adiabaticity parameter has real values for all field strengths, the modified adiabaticity parameter reaches a value of zero at the classical barrier suppression ionization (BSI) field strength (F_{BSI}) and is undefined for all greater field strengths. Above the BSI field strength, the molecule undergoes rapid ionization. Thus, the tunneling formulas determined with the zero range potential should be in ever increasing error as the field strength of the excitation source approaches and exceeds F_{BSI}. This is due not only to the significant difference in barrier length as determined by the two models but also to the substantial depression of the barrier height not accounted for in the zero range model. In the zero range model, the barrier height is equal to the ionization potential at all field strengths. We conclude that an adiabaticity parameter derived from a Coulomb potential is a more realistic descriptor of the ionization mechanism than models based on the zero range potential.

While an adiabaticity parameter calculated using a Coulomb potential does address the issue of structure in the electrostatic potential energy surface, the Coulomb potential does not accurately model the delocalized potentials associated with molecules, especially polyatomic species. We now consider the cases of more realistic molecular potentials (parts c and d of Figure 8) to describe the process of selecting origin location and axis orientation for arbitrary molecular potentials. A diatomic molecule is used to illustrate the application of the model employing an ab initio molecular potential. The choice of axes orientation for the diatomic case is determined by the bond axis, not only because this is the axis of highest symmetry

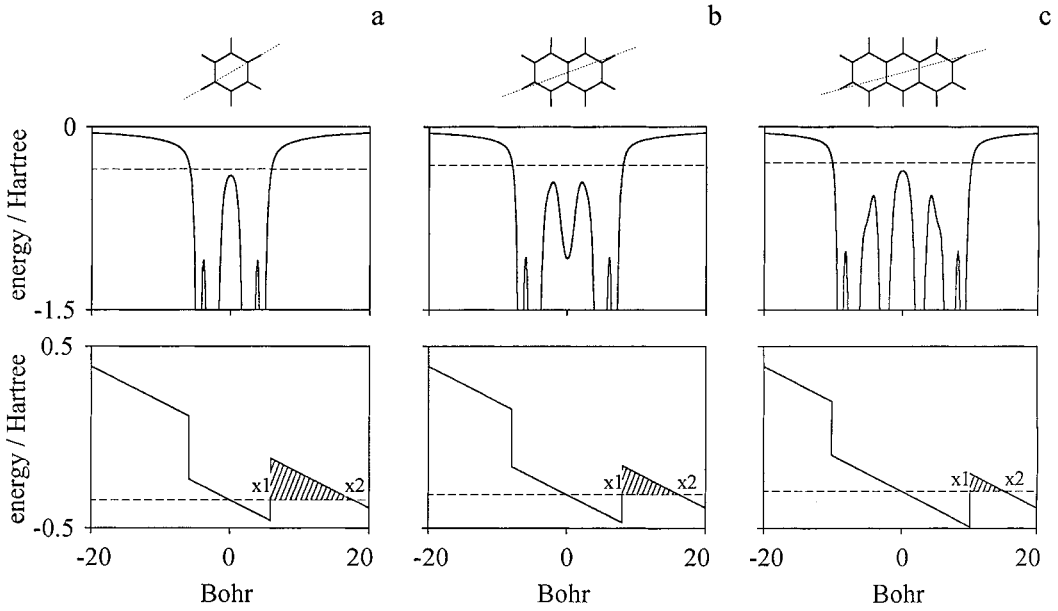

Figure 10. Schematics of the optimized geometries (from ab initio calculations) for (a) benzene, (b) naphthalene, and (c) anthracene. The dotted lines drawn on the molecular structures denote the axis employed for the one-dimensional electrostatic potentials extracted from the molecular wave function calculated using ab initio methods. Below each optimized geometry is plotted the optimal one-dimensional electrostatic potential employed for the adiabaticity calculations. The dashed lines represent the respective ionization potentials for the molecules. Below this is plotted the one-dimensional square-well approximation employed for the tunneling calculation of relative ionization probability. The depth of the rectangular well corresponds to the ionization potential of the molecule, and the width is the distance between the classical turning points defined by the ionization potential and the ab initio potential for each molecule. The electric field of the laser is superimposed to obtain the barrier to ionization.

but because it is the axis which most exemplifies the molecular character of the species: bonding and multiple charge centers.[19] However, a complication exists for molecular systems that was not present in the zero range and Coulomb derivations. As can be seen in parts c and d of Figure 8, the highest lying electron may or may not be free to move within the outer classical turning points of the unperturbed molecular potential. For this reason, the definition of the axis position for tunneling calculations must depend on the details of the molecular electrostatic potential. In the case of the strongly bound diatom depicted in Figure 8c, the origin would be located at the symmetry center and the tunneling axis would lie along the diatomic bond. Electrons are free to move between the outer classical turning points of the unperturbed molecular system so that an externally applied field can have a maximum effect on the developed barrier. The weakly bound diatom shown in Figure 8d, however, depicts a case in which a similarly placed tunneling axis would not define a path of free electron motion between outer classical turning points. In this case, when an external field is applied, it cannot be assumed to have the full effect on the bound electron. The weakly bound system might be expected to behave more like two independent atoms having lower tunnel probability than the strongly bound system.

The determination of axis orientation and origin position can be extended to arbitrarily large molecules. As long as the molecular symmetry is high, both the origin location and axis orientation can be chosen with confidence. A simple calculation of the molecular potential along the axis determines whether the orientation has only two classical turning points in the bound region of the potential, as in the case of Figure 8c, or if the orientation has multiple turning points as in the case of Figure 8d. Determining the appropriate one-dimensional potential involves searching through various orientations within the wave function to find the greatest distance between classical turning points.

The form of the potential used for an adiabaticity parameter calculation, whether zero range, Coulombic, or structure-based,

TABLE 1: Measured and Calculated Properties for Cyclic Aromatic Hydrocarbons

	benzene	naphthalene	anthracene
molecules	C_6H_6	$C_{14}H_{10}$	$C_{14}H_{10}$
ionization potential [eV]	9.386	8.575	8.045
γ [0.75 V Å^{-1}]	3.33	3.18	3.08
$\gamma(\psi)$ [0.75 V Å^{-1}]	1.95	1.30	0.47
calculated tunnel ionization probability, eq 12 [1.4 V Å^{-1}]	1	28	195
integrated ion yield [1.7 V Å^{-1}]	1	28	195
	1	20	200

has a significant impact on the predicted radiation−matter coupling mechanism for large polyatomic molecules.[17] Calculations of the structure-based adiabaticity parameters were carried out for the Xe, N_2, benzene, naphthalene, and anthracene as a function of the electric field strength of the laser, and the results are included in Figure 9. (The axes that determine the molecular potentials are in the plane of the nuclei and are depicted for benzene, naphthalene, and anthracene in the top panels of Figure 10.) Figure 9 reveals that the potential necessary for barrier suppression ionization is reduced in the structure-based model as compared to the Coulomb model. A direct comparison of the zero range Keldysh adiabaticity parameter and the structure-based adiabaticity parameter for benzene, naphthalene, and anthracene at 0.75 V Å^{-1} is included in Table 1, along with the pertinent physical characteristics of the molecules. The structure-based adiabaticity parameters are considerably lower than the zero range adiabaticity parameters[17,18,75,76] because of the previously detailed changes in the inner and outer turning point distances. This implies that molecules actually enter the tunneling regime at significantly lower laser powers in comparison to the zero range predictions. We note that the correction to the intensity required for field ionization is a lowering on the order of a factor of 10 or more for the molecules considered here. Finally, the adiabaticity parameters calculated using the molecular wave function are all below the value of 1 for the actual laser conditions employed in our laboratory, suggesting that the coupling mechanisms are all in the field ionization limit. The

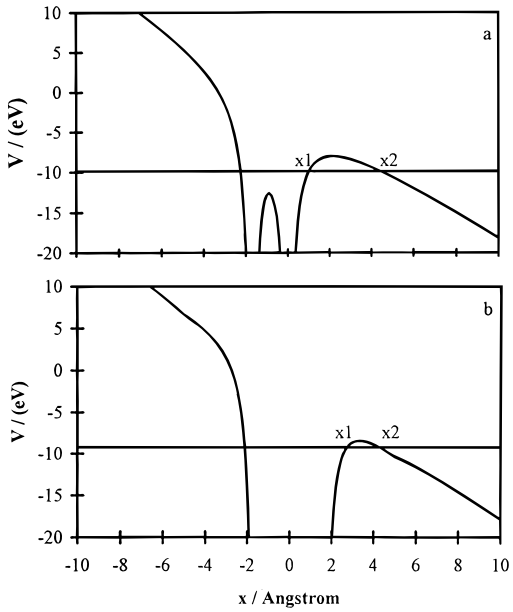

Figure 11. One-dimensional electrostatic potentials for (a) cyclohexane and (b) benzene along a C−C bond axis with the electric field (1.7 V Å^{-1}) superimposed.

zero range adiabaticity parameter suggests that MPI is operative for these molecules.

One value of the structure-based field ionization model is that a simple calculation of relative ionization probability can be performed. We can test whether the structure-based model is an accurate way to picture the excitation and ionization process by direct comparison of the predicted ionization rates with measurements of relative ion yields. Tunnel calculations are performed using the WKB approximation.[77] In this approximation, the tunneling rate, w, is given by

$$\text{rate} = e^{-W_0} \tag{13}$$

where

$$W_0 = 2\int_{r_1}^{r_2}(2[E - V(r)])^{1/2}\,dr \tag{14}$$

where E is the ionization potential of the system, $V(r)$ is the perturbed electrostatic potential, and x_1 and x_2 are the classical turning points determined by the ionization potential and the field-perturbed potential energy surface, as shown in Figure 11. For instance, the values of x_1 and x_2 bound the shaded region on the rectangular-well potential for each molecule as shown in Figure 10. To determine the potential, $V(r)$, we employ ab initio potentials generated at the Hartree−Fock level using a 6-311g++ basis set.[78] As an example of the influence of the electronic structure on the tunneling rate, the barriers calculated along a C−C bond axis in benzene and cyclohexane in an electric field of 1.7 V Å^{-1} are shown in Figure 11. Since the barrier resulting from the optimal one-dimensional potential for benzene is also smaller than that for cyclohexane, we predict, and indeed experimentally measure, a higher ionization probability for benzene in comparison with cyclohexane. The potential $V(r)$ can also be approximated by a rectangular well. In this approximation, the well has a width equal to the distance between the outer turning points of the optimal one-dimensional potential and a depth equivalent to the ionization potential. Examples for benzene, naphthalene, and anthracene are shown at the bottom of Figure 10. The relative tunnel rates calculated using eq 14 are included in Table 2 along with the experimental values. The experimentally measured ionization probabilities exhibit a ratio of 1:20:200 for benzene, naphthalene, and anthracene, respectively. These values are in reasonable agreement with the predictions of the tunneling model, 1:28:195 for benzene, naphthalene, and anthracene, respectively. Note that the tunneling calculation must be performed at a field strength that meets the requirements of the WKB approximation for all three molecules, $W_0 > 1$.[77] Thus, all of the molecules must remain in the tunnel ionization limit and the field strength must be less than F_{BSI}. For the cyclic aromatic series, we employed rectangular well approximation and a field strength of 1.4 V Å^{-1}.

TABLE 2: Measured and Calculated Relative Probabilities for C_6 Hydrocarbons

	benzene	1,3,5-hexatriene	cyclohexane	*n*-hexane
molecules	C_6H_6	C_6H_8	C_6H_{12}	C_6H_{14}
ionization potential [eV]	9.386	8.3	9.86	10.13
calculated tunnel ionization probability, eq 12 [1.2 V Å^{-1}]	1	69	0.13	7
integrated ion yield [1.7 V Å^{-1}]	1	79	0.15	N/A

The relative ionization probabilities for a number of other molecules have been predicted using this model, and in general, the agreement between the experimentally measured values and the calculations is found to be good. Published results include molecular series such as benzene, 1,3,5-hexatriene, cyclohexane, and hexane;[18] benzene, toluene, ethylbenzene, and *n*-propylbenzene;[56] benzene, naphthalene, and anthracene;[5,75] and several experiments being prepared for submission including acetylene, ethylene, and ethane;[79] 1,2-, 1,3-, and 1,4-benzenediol;[80] and benzene, biphenyl, diphenylmethane, and diphenylethane.[81] Two of the molecules in this list, *n*-hexane and *n*-propylbenzene, do not yield relative ionization probabilities which agree well with the model. However, these molecules undergo considerable dissociation under the experimental conditions, which is believed to have a tangible effect on the ultimate observable ion signal. Further experiments with shorter pulse duration lasers are underway to more fully investigate the competition between dissociation and ionization modes. The agreement between theory and experiment for such a wide variety of molecules lends credence to the hypothesis that the coupling mechanism is field mediated rather than MPI for the molecules under consideration here.

III.4. Photoelectron Spectroscopy. A stringent test of whether the radiation−molecule coupling mechanism is field- or MPI-mediated is found in the photoelectron kinetic energy distribution. This is particularly true for molecules where ionization occurs rapidly. In this case, the photoelectron spectrum is a signature of the events occurring during excitation and emission.[15,16,72,75] In the case of MPI in intense laser fields, one typically observes ATI, with a limited number of features displaying the periodicity of the photon energy are observed. The spectra display this simple appearance because the Stark shift of the intermediate states is exactly canceled by the acceleration of the liberated electron in the ponderomotive potential of the laser field. For sub-100 fs laser pulses, electrons cannot accelerate to the ponderomotive potential and the spectra can become quite complex. In the case of field ionization, a broad distribution is observed because of the indeterminacy in the precise time of tunneling in the laser cycle and the orientation of the molecule with respect to the electric field axis. Mevel

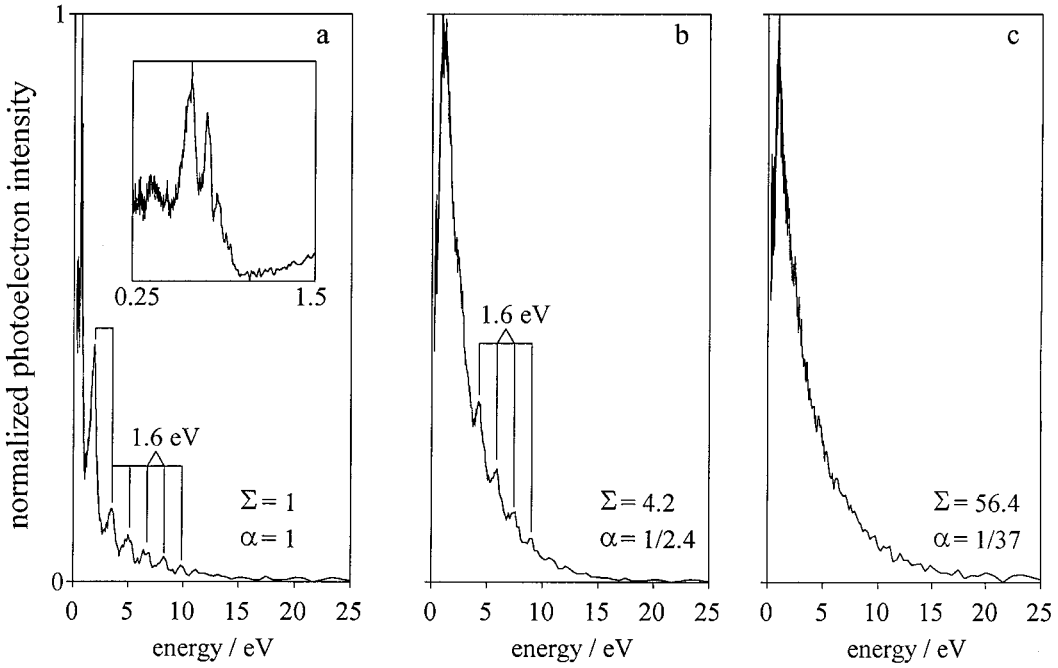

Figure 12. Photoelectron spectra for (a) benzene, (b) naphthalene, and (c) anthracene, measured using 3.8×10^{13} W cm^{-2} 780 nm radiation. The inset to panel a shows an expansion of the low-energy features for benzene. The scaling factor is shown as α, and the relative photoelectron intensity emitted along the laser beam polarization axis is shown as Σ.

and co-workers[15] used photoelectron spectroscopy to observe a transition from multiphoton to a field ionization in a series of noble gas atoms ranging from Xe to He. The transition was apparent in the fact that there were distinct MPI/ATI features observed in the Xe spectrum and the ATI/MPI features gradually disappeared as the ionization potential was increased through the series of target gases including Kr, Ar, Ne, and He. In the He photoelectron spectrum, no reproducible features were observed other than a broad featureless distribution extending to kinetic energies on the order of the ponderomotive potential of the laser pulse.

A similar transition from the multiphoton to field ionization regime has been observed by this laboratory in the series of molecules benzene, naphthalene, and anthracene.[75] The photoelectron spectra for these molecules are shown in Figure 12 after excitation using 780 nm radiation of duration 170 fs and intensity 3.8×10^{13} W cm^{-2}. The photoelectron spectrum for benzene, Figure 12a, displays a series of multiphoton features from 0.3 to 0.9 eV presumably due to ionization from the e_{1g} molecular orbital, and these features remain apparent to the lowest laser intensities employed. Above threshold ionization features separated by the photon energy, 1.59 eV, are observed from 2.5 to 15 eV. At the highest laser intensity, there are up to 8 ATI peaks. Also observable in the spectrum is a broad electron distribution ranging from 0 to 15 eV. This distribution is attributed to a field ionization mechanism. Deconvolution of the spectrum reveals that the contributions of multiphoton and field ionization represent 43% and 57% of the total electron current, respectively. The photoelectron spectrum for naphthalene taken at maximum laser intensity is shown in Figure 12b. Above threshold ionization features are again observed and are spaced by the photon energy with an integrated current at maximum laser intensity corresponding to approximately 14% of the total current. The photoelectron spectrum for anthracene, Figure 12c, reveals that from threshold to maximum laser intensity there are no discernible features other than the broad distribution. The broad feature simply increases in intensity and shifts to slightly higher kinetic energy (by 0.25 eV) as the laser intensity is increased. No discrete peaks attributable to MPI or ATI are observed at any intensity. The photoelectron distribution extends to approximately 20 eV in the case of anthracene.

The structure-based adiabaticity calculations for benzene, naphthalene, and anthracene, as described in section III.3 and summarized in Table 1, reveal that benzene has the largest value and anthracene the smallest. According to the definition of the adiabaticity parameter, this suggests that benzene should display the most MPI-like character and anthracene the least, in agreement with our observations. To gain some insight as to why benzene displays more MPI character and anthracene displays tunnel character, we consider the simple rectangular well model of the interaction of the electric field of the laser with the molecule. The one-dimensional rectangular wells shown in Figure 10 approximates the ab initio potential energy surface. Recall that the box width is related to the longest distance between classical turning points in the wave function and the box height is given by the ionization potential. The rectangular well has a 1 V/Å electric field superimposed to model the quasistatic laser field. As can be seen, the width of the rectangular well increases from benzene to naphthalene to anthracene. Note that the electric field of the laser has a greater influence on the barrier to tunneling as the width of the rectangular well increases. This results in a anthracene having the smallest barrier to tunnel ionization in comparison naphthalene and benzene. Thus, we predict that the probability for tunneling should be markedly enhanced for anthracene in comparison to benzene. This prediction is consistent with both the photoelectron distributions and the relative intensities of the photoelectron spectra displayed in Figure 12. Anthracene displays the most tunneling character and benzene the least. Note that, qualitatively, a photoelectron spectrum displaying a featureless distribution extending above the laser's ponderomotive potential is a hallmark of the field ionization regime.[15,16]

The field strength for barrier suppression ionization can be calculated using molecular potentials and compared with values from the Coulomb potential. We calculate a value of F_{BSI} of 1.27 V Å^{-1} for the structure-based method vs a value of 1.53

V Å^{-1} for a Coulomb potential in the case of benzene, 0.98 V Å^{-1} vs 1.28 V Å^{-1} for naphthalene, and 0.78 V Å^{-1} vs 1.12 V Å^{-1} for anthracene. In the series benzene, naphthalene, and anthracene, the field strength corresponding to the onset of barrier suppression ionization calculated using the structure-based potential is an increasingly smaller fraction of that calculated using the Coulomb potential. This suggests that molecules with delocalized electronic orbitals enter the field ionization regime at much lower intensities than those predicted using the zero range model. This is also in agreement with the photoelectron measurements.

At this point, it might be worth noting that the two previously accepted models (the zero range and the Coulomb) for atomic potentials interacting with intense lasers lead to a logical inconsistency when directly applied to large molecular systems. At 1.7 V Å^{-1}, the highest field strength employed in this study, the Keldysh adiabaticity parameter predicts that a multiphoton mechanism is responsible for benzene ionization, yet the common expression for F_{BSI} derived for Coulomb potentials predicts that barrier suppression ionization occurs at all field strengths above 1.53 V Å^{-1}. This also suggests that more accurate descriptions are required to model the interaction of intense lasers with polyatomic molecules.

III.5. Intense Laser−Molecule Photodissociation Mechanisms. There are two questions that are apparent from the mass spectra presented thus far. The first concerns identification of the mechanisms leading to dissociation of polyatomic molecules in intense laser fields. Possible mechanisms contributing to dissociation include ADI and AID and may involve field-induced processes. The second question concerns the mechanism by which some molecules survive intact in laser fields approaching 10^{14} W cm^{-2}. The pulse duration of the laser is certainly short enough to decrease the probability of a molecule undergoing neutral dissociation before excitation above the ionization potential. However, even if such ADI or ladder switching mechanisms are suppressed, one expects the AID mechanism to be active in these intense laser pulses. This is because the photon density is sufficient to drive excitation of the ion to higher lying states, some of which may be dissociative. A calculation of the photon density reveals that the number of photons per cubic wavelength is on the order of 3×10^9 in the 170 fs pulse employed in these investigations. This is many orders of magnitude greater than the photon densities found in nanosecond pulses employed for two or three photon resonant excitation, for instance. This fact suggests that multiphoton excitation of the ion should be facile. Thus, one might expect correspondingly higher dissociation yields with the higher laser intensities available using femtosecond pulses, but this is not observed. As another example of nonintuitive behavior in the dissociation of molecules in intense laser fields, Willey et al.[59] found a *decrease* in the measured dissociation yield upon *increasing* the intensity of a laser while maintaining the pulse duration at 2 ps. This phenomenon was observed in the photoionization of $Cr(CO)_6$ over an intensity range $10^{12}-10^{13}$ W cm^{-2}. To begin to elucidate the photodissociation mechanisms present during intense near-infrared excitation, we summarize three experiments that have been performed in our laboratory. The first involves measuring the dissociation probability for a series of alkyl-substituted benzenes. The second involves an investigation of the dissociation probability for a series of C_6 hydrocarbons having a varying degree of saturation, and the last involves measuring the dissociation yield for a series of aromatic hydrocarbons.

The dissociation probability for a series of alkyl-substituted benzene molecules was measured to understand the role of increasing vibrational degrees of freedom on the ionization/dissociation probability. We anticipated that, as the density of states in the target molecule increased (by increasing the degrees of freedom), the dissociation branching ratio would decrease. As will be seen, this hypothesis was not consistent with the experimental observations. Fluorescence measurements have demonstrated that the rate of intramolecular vibrational energy redistribution (IVR) increases considerably as the length of the alkyl substituent is increased.[82] Measurements of the intense 780 nm laser ionization/dissociation of C_6H_5X, where X = −H, $-CH_3$, $-CH_2CH_3$, $-CH_2CH_2CH_3$,[56] at 3.8×10^{13} W cm^{-2} are shown in Figure 13. The spectra revealed two trends as the length of the substituent was increased. The first was an increase in the dissociation yield with increasing number of atoms contained in the molecule. The dissociation yield increased with the number of atoms in the molecule approximately as $(N - 12)^2$, where N is the number of atoms and 12 represents the number of atoms in benzene, displaying virtually no dissociation. The dissociation trend suggests that the energy transfer to nuclear degrees of freedom is enhanced in the larger molecules. One mechanism for this would be an increase in energy deposition into the molecule with increasing alkyl chain length. Such a trend is predicted by the field-mediated coupling mechanism because the distance between classical turning points in the optimal one-dimensional potential increases from benzene to *n*-propylbenzene. Note that in weak field excitation the relative electronic transition moments are reasonably constant in the first absorption band for these molecules ($\sim$250l mol^{-1} cm^{-1}). The second major observation from the study was that, as the alkyl chain length increased from two to three carbon units, the photoionization probability decreased precipitously. This may be attributed to an increase in the channeling of excitation energy into dark photodissociation modes. This may also be due to the increasing degree of σ-type bonding in the series benzene, toluene, ethylbenzene, and *n*-propylbenzene, or it may be due to exciting dissociative states in the larger molecules. Further photoelectron measurements are necessary to understand the trends observed as a function of the change in the degree of σ-bonding in a molecule.

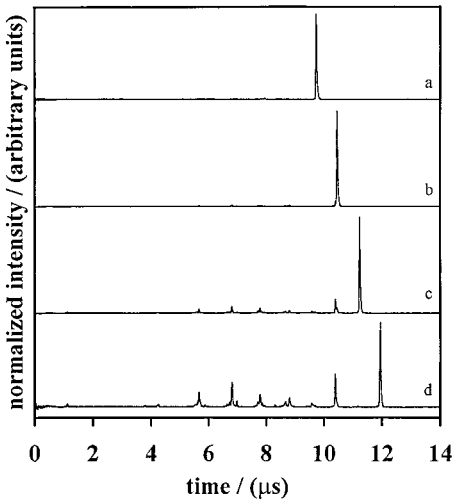

Figure 13. Time-of-flight mass spectra for (a) benzene, (b) toluene, (c) ethylbenzene, and (d) *n*-propylbenzene ionized using 3.8×10^{13} W cm^{-2} 780 nm radiation of duration 170 fs.

An intriguing observation from the alkylbenzene study is the fact that ion signal is generated at C_3, C_4, and C_5 species for ethylbenzene and at C_4 and C_5 species for *n*-propylbenzene. These mass features imply that at least two aromatic bonds are

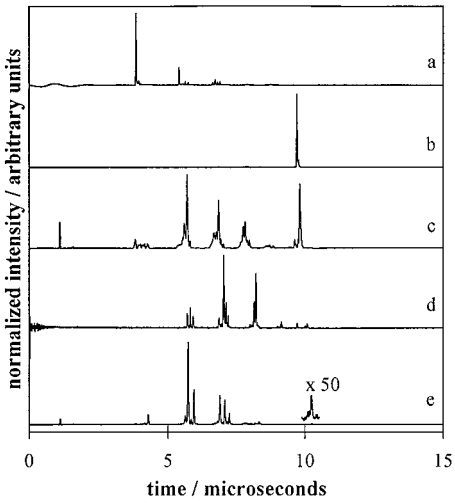

Figure 14. Time-of-flight mass spectra for (a) benzene ionized using 10^{11} W cm^{-2} 532 nm radiation of duration 4 ns, (b) benzene, (c) 1,3,5-hexatriene, and (d) cyclohexane ionized using 3.8×10^{13} W cm^{-2} 780 nm radiation of duration 170 fs. Panel e displays the mass spectrum for *n*-hexane photoionized using a 125 fs laser pulse of similar energy to that used in (a−d).

being broken during or after the excitation and ionization step. One possible explanation for the additional fragmentation in the larger alkylbenzene species might simply be the increased proportion of weaker C−C single bonds in these molecules. Such bonding may increase the probability of pumping through or to dissociative states during excitation. There is little doubt that such a mechanism plays a role in the dissociation observed, but this mechanism alone cannot explain the presence of the fragments noted above for ethyl and *n*-propylbenzene. A substantial amount of energy must be coupled into the very stable aromatic ring to cleave a pair of double bonds to produce the ions listed previously. We have proposed that a new mechanism involving the production of energetic electrons within the molecule may account for the observed dissociation. In this mechanism, the dissociation yield is mediated by the electronic polarization of the molecule as produced by the electric field of the laser.[18] This polarization increases with increasing alkyl chain length. Energy stored in such electronic polarization can be transferred to the nuclear modes both during and after the laser pulse via field-induced curve crossings, field-induced proton migration, and Coulomb repulsion between positively charged nuclei in the center of the molecule. Further support for a field-mediated dissociation mechanism was obtained from measuring the photoionization/dissociation probability of a series of hydrocarbons where the bonding type changes, but the number of carbon atoms in the molecule remains constant as described next.

To investigate the influence of the type of chemical bonding on the photodissociation yield, mass spectra for a series of C_6H_x ($x = 6-14$) hydrocarbons were recorded as a function of laser intensity using intense 780 nm excitation, 170 fs duration.[18] The series of molecules included benzene, 1,3,5-hexatriene, cyclohexane, and *n*-hexane. The photoionization spectra measured at 3.8×10^{13} W cm^{-2} are shown in parts b, c, and d of Figure 14 for benzene, 1,3,5-hexatriene, and cyclohexane, respectively. Note that, as the fraction of σ-bonding in the molecule increases, so does the yield of dissociated ions. For this series, as the laser intensity is decreased, the photodissociation distribution shifts toward the intact parent ion peak. No ion intensity was observed for the molecule *n*-hexane at any laser intensity employed using the 170 fs duration laser. The fact that *n*-hexane is not observed suggests that photodissociation channels in the linear alkane dominate the photoexcitation process. This result is in accord with the alkylbenzene investigation detailed previously in that the ion yield was reduced when the alkyl chain length increased to *n*-propylbenzene. Recently, a shorter duration (125 fs) laser pulse was employed to enhance the ionization rate over the presumably rapid dissociation rate and indeed substantial dissociation/ionization was detected in *n*-hexane as shown in Figure 14e. We conclude that the longer alkyl chains promote efficient channeling of electronic energy into nuclear motion. The distributions can be quantitatively analyzed using the ratio of the integrated fragment ion intensity and the parent ion intensity. For this series, we again observed a significant increase in the photodissociation yield as the degree of σ-bonding increased. Also, there may be evidence for energetic dissociation in 1,3,5-hexatriene because C_1^+, C_3^+, and C_5^+ ion species are observed. These species would not be expected if the mechanism for dissociation was simply fragmentation of the weaker σ-bonds in comparison to the stronger C=C double bonds. Electronic structure calculations of the radical cation would provide additional insight into this dissociation mechanism. Another mechanism of dissociation would be absorption of additional photons by the ion (AID). Analysis of the one-photon photoelectron spectrum reveals that lowest order absorption cannot account for the observed dissociation trends because there is no 780 nm resonance. In other words, there is no feature in the spectrum of either benzene or 1,3,5-hexatriene 1.59 eV above the ground-state ion feature. There is a broad continuum in the HeI photoelectron spectrum of cyclohexane extending 6 eV above the ionization potential that may contribute to the dissociation in this molecule.

Further evidence for a field-induced dissociation mechanism can be found in a comparison of the kinetic energy distributions of the dissociation products after ionization for molecules that ionize through a field mechanism versus a multiphoton mechanism.[18] For instance, in the mass spectrum shown in Figure 13c, the resolution of the mass spectrum degrades for the lighter masses in the case of 1,3,5-hexatriene, a molecule that presumably undergoes field ionization. Various features have been analyzed in the mass spectrum of cyclohexane, a candidate for MPI, and the resolution is constant and on the order of $200m/\Delta m$. For the molecule 1,3,5-hexatriene, the resolution degrades from a maximum of 150 for the parent ion to 100 for the intermediate fragments to approximately 40 for the H^+ ions. A similar distribution in resolution has been observed for other molecules, naphthalene for example. The degradation in resolution suggests that some form of kinetic energy release is occurring upon dissociation/ionization. The kinetic energy distribution can be calculated by deconvoluting the H^+ feature, and we estimate that the total kinetic energy release is on the order of 20 eV. Trushin and co-workers have observed a similar kinetic energy distribution for the molecule 1,3,5-hexatriene and attribute the phenomenon to Coulomb explosion.[64] However, in the measurements performed in our laboratory, there is little evidence for the multiple charging necessary for the Coulomb explosion mechanism. We attribute the kinetic energy release observed in the mass spectra to a field-induced process. The spread in kinetic energy is most likely not due to metastable decay because of the presence of a splitting in the H^+ peak that is consistent with forward and backward scattered distributions occurring in a well-defined region in space. The precise mechanism of this field-induced dissociation/ionization is under investigation at the present time.

We have investigated a series of robust cyclic aromatic

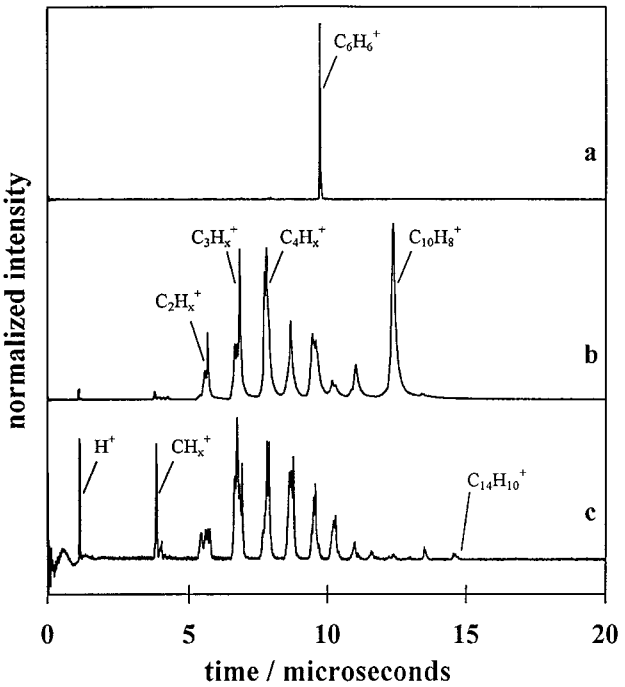

Figure 15. Comparison of the intense near-infrared laser ionization time-of-flight mass spectra measured for the molecules (a) benzene, (b) naphthalene, and (c) anthracene using 3.8×10^{13} W cm^{-2} 780 nm radiation.

hydrocarbons to attempt to separate the contributions of σ-bonding and polarizability to the dissociation process. In the series benzene, naphthalene, and anthracene, the polarizability changes markedly and no additional C−C σ-bonding is introduced across the series. The polarizability increases across this series from 10.5 to 16.5 to 25.4 Å^3. The mass spectra for benzene, naphthalene, and anthracene at a moderate laser intensity are shown in Figure 15. The polarization possible with electric fields on the order of several V Å^{-1} is substantial and increases with the number of rings in these aromatic hydrocarbons. The field-induced electronic polarization leads to massive Stark shifting and field-induced curve crossings both in the excited neutral and ionic states. It is important to note that each of these molecules is relatively robust to nanosecond resonance-enhanced multiphoton ionization in comparison to substituted aromatics, for example. In fact, anthracene is commonly employed for analytical REMPI of rather exotic samples, extraterrestrial rocks, for instance.[83] Upon exposure to the intense radiation field, the photodissociation probability again increases significantly for the series benzene, naphthalene, and anthracene. For the molecule benzene, only minor dissociation/ionization is observed at any laser intensity up to 4×10^{13} W cm^{-2}. For the molecule naphthalene, an increasing degree of dissociation/ionization is measured as shown in Figure 5. Until highest laser intensity, the intact parent naphthalene peak is the most intense feature in the spectrum. For the case of anthracene, substantially enhanced dissociation/ionization is observed at all laser intensities and the parent ion is not the dominant peak in the mass spectrum until the lowest laser intensities are employed ($\sim 1 \times 10^{13}$ W cm^{-2}). This trend of increasing dissociation/ionization is consistent with a model that incorporates the electronic polarization during intense laser excitation. Again, the increase in dissociation may also be consistent with a simple increase in the rate of AID due to the increased density of states in the ionic states of larger molecules. However, for these molecules, such a trend is not obvious in corresponding nanosecond experiments. Nor are there resonances in any of the molecules in the ion states for one photon absorption from the lowest energy ion state in the HeI photoelectron spectra. It is also of note that considerably larger molecules, such as laser vaporized Rh6G, can be ionized with limited accompanying decomposition. This latter observation suggests that the dissociation probability is not simply dependent on the degrees of freedom, density of states, or size of the molecule.

Summary

An overview of the interaction of intense, near-infrared laser pulses with polyatomic molecules has been presented. We describe both ion and photoelectron spectroscopic data to shed light on the coupling mechanisms between a polyatomic molecule and radiation at intensities where the electric field of the laser approaches the fields binding valence electrons to nuclei. We demonstrated that, for a variety of molecules, some fraction of the ion current is found as the intact molecular ion. This suggests the possibility of a widely applicable, nonresonant ionization method. We presented measurements of relative ionization probabilities for well-defined series of molecules and found that the ionization probability increases both with decreasing ionization potential and increasing spatial extent or "size" as defined by the distance between classical turning points in the electronic potential energy surface.

The measurements of relative ionization probabilities were rationalized using a structure-based tunnel ionization model. Limitations in the application of zero range and Coulomb-based field ionization models to polyatomic molecules were identified and a detailed description of the structure-based model was presented. In this model an optimal one-dimensional electrostatic potential is employed for both adiabaticity parameter calculations and for determining relative tunneling rates. The optimal potential is defined as that one-dimensional electrostatic potential in the molecular wave function that has the greatest distance between classical turning points at the ionization potential. The predictions of the structure-based model were compared to the measured relative ionization probabilities for several series of molecules. Good agreement was found for all series as dissociation channels dark to ion detection do not dominate the interaction. The agreement between the model and experimental measurements suggested that the field ionization is the dominant mechanism under the conditions employed here.

The predictions of the structure-based model were further tested by measuring the photoelectron spectra for benzene, naphthalene, and anthracene. We observed that the mechanism of coupling changed from a mixed multiphoton field to field dominated as the spatial size of the molecule increased from benzene to anthracene. This transition was accurately predicted by the structure-based adiabaticity parameter, while the zero range adiabaticity parameter predicted all molecules to remain in the MPI regime.

The mechanisms of photodissociation in intense ultrafast laser fields were also discussed. It was found that the number of degrees of freedom, the degree of σ-type bonding, and polarizability of the molecule correlated to increasing dissociation. We have proposed that a photoionization/dissociation model based on transfer of energy from electronic to nuclear modes via a polarization mechanism may account for the qualitative trends observed.

Acknowledgment. We acknowledge the support of the National Science Foundation through a Young Investigator Award (R.J.L.). The support of the Sloan and Dreyfus Foundations is also greatly appreciated. The authors acknowledge the

assistance of Noel P. Moore in the construction of the photoelectron spectrometer. The Chemistry Department at the University of Cambridge is also acknowledged for support during the completion of this article. Finally, we thank the reviewers for stimulating comments.

References and Notes

(1) L'Huillier, A.; Lompré, L. A.; Mainfray, G.; Manus, G. *Atoms in Intense Laser Fields*; Gavrilla, M., Ed.; Academic Press: Boston, 1993; pp 137−206.
(2) Agostini, P. F.; Fabre, F.; Mainfray, G.; Petite, G.; Rahman, N. K. *Phys. Rev. Lett.* **1979**, *2*, 1127.
(3) Zavriyev, A.; Bucksbaum, P. H.; Squier, J.; Saline, F. *Phys. Rev. Lett.* **1993**, *70*, 1077.
(4) Frasinski, L. J.; Codling, K.; Hatherly, P. A.; Barr, J.; Ross I. N.; Toner, W. T. *Phys. Rev. Lett.* **1987**, *58*, 2424.
(5) DeWitt, M. J.; Levis, R. J. *J. Chem. Phys.* **1995**, *102*, 8670.
(6) Chelkowski, S.; Conjusteau, A.; Zuo, T.; Bandrauk, A. D. *Phys. Rev A.* **1996**, *54*, 3235.
(7) Cornaggia, C.; Normand, D.; Morellec, J.; Mainfray, G.; Manus, C. *Phys. Rev. A* **1986**, *34*, 207.
(8) Verschuur, J. W. J.; Noordam, L. D.; van dan Linden van den Heuvell, H. B. *Phys. Rev. A* **1989**, *40*, 4383.
(9) Wu, M.; Taylor, D. P.; Johnson, P. M. *J. Chem. Phys.* **1991**, *94*, 7596.
(10) Keldysh, L. V. *Sov. Phys. JETP* **1965**, *20*, 1307.
(11) Perelomov, A. M.; Popov, V. S.; Terent'ev, M. V. *Sov. Phys. JETP* **1966**, *23*, 924−934.
(12) Ammosov, M. V.; Delone, N. B.; Krainov, V. P. *Sov. Phys. JETP* **1986**, *91*, 1191−1194.
(13) Augst, S.; Strickland, D.; Meyerhofer, D. D.; Chin, S. L.; Eberly, J. H. *Phys. Rev. Lett.* **1989**, *63*, 2212.
(14) Walsh, T. D. G.; Ilkov, F. A.; Decker, J. E.; Chin, S. L. *J. Phys. B* **1994**, *27*, 3767.
(15) Mevel, E.; Breger, P.; Trainham, R.; Petite, G.; Agostini, P.; Migus, A.; Chambaret, J. P.; Antonetti, A. *Phys. Rev. Lett.* **1993**, *70*, 406.
(16) Corkum, P. B.; Burnett, N. H.; Brunel, F. *Phys. Rev. Lett.* **1989**, *62*, 1259.
(17) DeWitt, M. J.; Levis, R. J. *J. Chem. Phys.* **1998**, *108*, 7739.
(18) DeWitt, M. J.; Levis, R. J. *J. Chem. Phys.* **1998**, *108*, 7045.
(19) Brewczyk, M.; Frasinski, L. J. *J. Phys. B: At. Mol. Opt. Phys.* **1991**, *24*, L307.
(20) Strickland, D. T.; Beaudoin, Y.; Dietrich, P.; Corkum, P. B. *Phys. Rev. Lett.* **1992**, *68*, 2755.
(21) Deitrich, P.; Corkum, P. B. *J. Chem. Phys.*. **1992**, *97*, 3187.
(22) Normand, D.; Cornaggia, C.; Lavancier, J.; Morellec, J.; Liu, H. X. *Phys. Rev. A* **1991**, *44*, 475.
(23) Cornaggia, C.; Lavancier, J.; Normand, D.; Morellec, J.; Agostini, P.; Chambaret, J. D.; Antonetti, A. *Phys. Rev. A* **1991**, *44*, 4499.
(24) Codling, R.; Cornaggia, C.; Frasinski, L. J.; Hatherly, P. A.; Morellec, J.; Normand, D. *J. Phys. B: At. Mol. Opt. Phys.* **1991**, *24*, L593.
(25) Zavriyev, A.; Bucksbaum, P. H.; Muller, H. G.; Schumacher, D. W. *Phys. Rev. A* **1990**, *42*, 5500.
(26) Zavriyev, A.; Bucksbaum, P. H.; Squier, J.; Saline, F. *Phys. Rev. Lett.* **1993**, *70*, 1077.
(27) Yang, B.; Saeed, M.; DiMauro, L. F.; Zavriyev, A.; Bucksbaum, P. H. *Phys. Rev. A* **1991**, *44*, R1458.
(28) Yu, H.; Zuo, T.; Bandrauk, A. B. *J. Phys. B: At. Mol. Opt. Phys.* **1998**, *31*, 1. Yu, H.; Bandrauk, A. D. *Phys. Rev.* **1997**, *56*, 685.
(29) Zuo, T.; Bandrauk, A. D. *Phys. Rev. A* **1995**, *52*, 1.
(30) Schmidt, M.; Normand, D.; Cornaggia, C. *Phys. Rev. A* **1994**, *50*, 5037.
(31) Cornaggia, C.; Schmidt, M.; Normand, D. *J. Phys. B: At. Mol. Opt. Phys.* **1994**, *27*, L123.
(32) Hatherly, P. A.; Stankiewicz, M.; Codling, K.; Frasinski, L. J.; Cross, G. M. *J. Phys. B: At. Mol. Opt. Phys.* **1994**, *27*, 2993.
(33) Cornaggia, C.; Schmidt, M.; Normand, D. *Phys. Rev. A* **1995**, *51*, 1431. Cornaggia, C.; Normand, D.; Morellec, J. *J. Phys. B: At. Mol. Opt. Phys.* **1992**, *25*, L415.
(34) Cornaggia, C. *Phys. Rev. A* **1995**, *52*, R4328.
(35) Echt, O.; Morgan, P. D.; Dao, S.; Stanley, R. J.; Castleman, A. W. *Ber. Bunsen Ges. Phys. Chem.* **1984**, *88*, 217.
(36) Cao, H. Z.; Evleth, E. M.; Kassab, E. J. *Chem. Phys.* **1984**, *81*, 1512.
(37) Gaspard, P.; Burghardt, I., Eds. *Chemical Reactions and Their Control on the Femtosecond Timescale*; Wiley: New York, 1997.
(38) Gobeli, D. A.; Morgan, J. R.; St. Pierre, R. J.; El-Sayed, M. A. *J. Phys. Chem.* **1984**, *88*, 178.
(39) Szaflarski, D. M.; Chronister, E. L.; El-Sayed, M. A. *J. Phys. Chem.* **1987**, *91*, 3259.
(40) Szaflarski, D. M.; El-Sayed, M. A. *J. Phys. Chem.* **1988**, *92*, 2234.
(41) Wilkinson, C. W.; Reilly, J. P. *Anal. Chem.* **1990**, *62*, 1804.
(42) Wilkinson, C. W.; Colby, S. M.; Reilly, J. P. *Anal. Chem.* **1989**, *61*, 2669.
(43) Wei, S.; Purnell, J.; Buzza, S.; Stanley, R. J.; Castleman, A. W. *J. Chem. Phys.* **1992**, *97*, 9480.
(44) Baumert, T.; Grosser, M.; Thalweiser, R.; Gerber, G. *Phys. Rev. Lett.* **1991**, *67*, 3753.
(45) Wei, S.; Tzeng, W. B.; Castleman, A. W. *J. Chem. Phys.* **1990**, *93*, 2506.
(46) Lin, C. H.; Matsumoto, J.; Ohtake, S.; Imasaka, T. *Talanta* **1996**, *43*, 1925.
(47) Matsumoto, J.; Lin, C. H.; Imasaka, T. *Anal. Chem.* **1997**, *69*, 4524.
(48) Terhost, M.; Mollens, R.; Niehuis, E.; Benninghoven, A. *Surf. Interface Anal.* **1992**, *18*, 824.
(49) Weinkauf, R.; Aicher, P.; Wesley, G.; Grotemeyer, J.; Schlag, E. W. *J. Phys Chem.* **1994**, *98*, 8381.
(50) Stuke, M. *Appl. Phys. Lett.* **1984**, *45*, 1175.
(51) Larciprete, R.; Stuke, M. *J. Cryst. Growth* **1986**, *77*, 235.
(52) Stuke, M. *Appl. Phys. Lett.* **1984**, *45*, 1175.
(53) Ledingham, K. W. D.; Kosmidis, C.; Georgiou, S.; Couris, S.; Singhal, R. P. *Chem. Phys. Lett.* **1995**, *247*, 555.
(54) Banares, L.; Baumert, T.; Bergt, M.; Kiefer, B.; Gerber, G. *J. Chem. Phys.* **1988**, *108*, 5799.
(55) Zewail, A. H. *Femtochemistry-Ulrafast Chemical and Physical Processes in Molecular Systems*; World Scientific: Singapore, 1994.
(56) DeWitt, M. J.; Peters, D. W.; Levis, R. J. *Chem. Phys.* **1997**, *218*, 211.
(57) DeWitt, M. J.; Levis, R. J. In *Femtochemistry, Ultrafast Chemical and Physical Processes in Molecular Systems*; Chergui, M., Ed.; World Scientific: Singapore, 1996; pp 129−134.
(58) Levis, R. J.; DeWitt, M. J. In *Resonance Ionization Spectroscopy*; Winograd, N., Ed.; AIP Press: New York, 1997; pp 45−50.
(59) Willey, K. F.; Brummel, C. L.; Winograd, N. *Chem. Phys. Lett.* **1997**, *267*, 359.
(60) Ledingham, K. W. D.; Singhal, R. P. *Int. J. Mass Spectrom. Ion Processes* **1997**, *163*, 149.
(61) Singhal, R. P.; Kilic, H. S.; Ledingham, K. W. D.; Kosdimis, C.; McCanny, T.; Langley, A. J.; Shaikh, W. *Chem. Phys. Lett.* **1996**, *253*, 81.
(62) Baumert, T.; Gerber, G. *Phys. Scr.* **1997**, *T72*, 53−68.
(63) Trushin, S. A.; Fuss, W.; Schikarski, T.; Schmid, W. E.; Kompa, K. L. *J. Chem. Phys.* **1997**, *106*, 9386.
(64) Fuss, W.; Kompa, K. L.; Schikarski, T.; Schmid, W. E.; Trushin, S. A. In *SPIE Proceedings, 3271: Conference on Laser Techniques for State Selected and State-to-State Chemistry IV*; Hepburn, J., Ed.; AIP Press: New York, 1998.
(65) Trushin, S. A.; Fuss, W.; Schmid, W. E.; Kompa, K. L. *J. Phys. Chem. A* **1998**, *102*, 4124.
(66) Castillejo, M.; Couris, S.; Koudoumas, E.; Martin, M. *Chem. Phys. Lett.* **1998**, *289*, 303.
(67) Spence, D. E.; Rean, P. N.; Sibbe, W. *Opt. Lett.* **1991**, *16*, 42.
(68) Squier, J.; Salin, F.; Mourou, G.; Harter, D. *Opt. Lett.* **1991**, *16*, 324.
(69) Letokhov, V. S. *Laser Photoionization Spectroscopy*; Academic Press: New York, 1981.
(70) Pan, L.; Armstrong, L., Jr.; Eberly, J. H. *J. Opt. Soc. B* **1986**, *3*, 1319.
(71) Kibble, T. W. *Phys. Rev.* **1966**, *150*, 1060.
(72) Bucksbaum, P. H.; Freeman, R. R.; Bashkansky, M.; McIlrath, T. J. *J. Opt. Soc B* **1987**, *4*, 760.
(73) Avon, P.; Cohen-Tannoudji, C.; Dupont-Roc, J.; Fabre, C. *J. Phys. (Paris)* **1976**, *37*, 993.
(74) Ammosov, M. V.; Delone, N. B.; Krainov, V. P. *Sov. Phys. JETP* **1986**, *91*, 1191.
(75) DeWitt, M. J.; Levis, R. J. *Phys. Rev. Lett.* **1998**, *81*, 5101.
(76) DeWitt, M. J.; Levis, R. J. *J. Chem. Phys.*, in press.
(77) Bohm, D. *Quantum Theory*; Prentice Hall: New York, 1951.
(78) Frisch, M. J.; Trucks, G. W.; Head-Gordon, M.; Gill, P. M. W.; Wong, M. W.; Foresman, J. B.; Johnson, B. G.; Schlegel, H. B.; Robb, M. A.; Replogle, E. S.; Gomperts, R.; Andres, J. L.; Raghavachari, K.; Binkler, J. S.; Gonzales, C.; Martin, R. T.; Fox, G. J.; Defrees, D. J.; Baker, J.; Stewart, J. J. P.; Pople, J. A. *Gaussian 95*; Gaussian, Inc.: Pittsburgh, PA, 1995.
(79) Prall, B. S.; DeWitt, M. J.; Levis, R. J. *J. Chem. Phys.* **1999**, *111* (7).
(80) DeWitt, M. J.; Prall, B. S.; Levis, R. J. Submitted.
(81) Billotto, R.; Levis, R. J. Submitted.
(82) Hopkins, J. B.; Powers, D. E.; Smalley, R. E. *J. Chem. Phys.* **1980**, *72*, 5039.
(83) McKay, P. S.; Gibson, E. K.; Thomas-Keptra, K. L.; Vali, H.; Romanek, C. S.; Clemett, S. J.; Chillie, X. D. F.; Maechling, C. R.; Zare, R. N. *Science* **1996**, *273*, 924.